Pre-Assessment of Transtibial Prosthetic Pylon Using Auxetic Bowtie Model: A Simulation and Experimental Validation

Bhre Wangsa Lenggana
Department of Mechanical Engineering, Faculty of Engineering, Universitas Sebelas Maret, Surakarta, Indonesia
bhrewangsa20@gmail.com

Muhammad Faris Fardan
Department of Mechanical Engineering, Faculty of Engineering, Universitas Sebelas Maret, Surakarta, Indonesia
farisfardan21@student.uns.ac.id

Ubaidillah
Department of Mechanical Engineering, Faculty of Engineering, Universitas Sebelas Maret, Surakarta, Indonesia
ubaidillah_ft@staff.uns.ac.id (corresponding author)

Seung-Bok Choi
Department of Mechanical Engineering, The State University of New York, Korea (SUNY Korea), Incheon, South Korea | Department of Mechanical Engineering, Industrial University of Ho Chi Minh City (IUH), Ho Chi Minh City, Vietnam
seungbok.choi@sunykorea.ac.kr

Didik Djoko Susilo
Department of Mechanical Engineering, Faculty of Engineering, Universitas Sebelas Maret, Surakarta, Indonesia
djoksus@gmail.com

Sohaib Zia Khan
Mechanical Engineering Department, Faculty of Engineering, Islamic University of Madinah, Al Madinah Al Munawwarah, Saudi Arabia | King Salman Center for Disability Research, Riyadh, Saudi Arabia
szkhan@iu.edu.sa

Asad Ali Zaidi
Mechanical Engineering Department, Faculty of Engineering, Islamic University of Madinah, Al Madinah Al Munawwarah, Saudi Arabia | King Salman Center for Disability Research, Riyadh, Saudi Arabia
sali@iu.edu.sa

Received: 21 August 2025 | Revised: 11 September 2025 and 17 September 2025 | Accepted: 20 September 2025

 DOI: https://doi.org/10.48084/etasr.14213

ABSTRACT

In the present study, a prosthetic device is designed to function as a replacement for a missing limb. This device typically consists of suspension, liner, socket, pylon, and foot components. The research objectives are to design a pylon component for transtibial prosthetics by implementing auxetic metamaterials and to validate the performance of the designed pylon under quasi-static and dynamic conditions. The design and analysis processes were conducted with Finite Element Analysis (FEA), and its effectiveness was validated through experimental testing of the prototype pylon sample. In the design process, the pylon structure is formulated by rearranging the Two-Dimensional (2D) re-entrant hexagon model into a Three-Dimensional (3D) model. The design evaluation identified that the pylon exhibits a stiffness of 1404 kN/mm, 4680 kN/mm, and 9360 kN/mm for the 0.3 mm, 1 mm, and 2 mm thick ligaments, respectively. It was found that a pylon with a 0.3 mm-thick ligament caused a deformation (S) of 0.53 cm during a single period of the gait cycle, while a 1 mm-thick ligament caused an S of 0.4 cm. It was also found from the S transition of the primary and secondary bends that a negative Poisson's ratio occurred in the 3D model transformed from a 2D re-entrant hexagon.

Keywords-transtibial prosthetics; auxetic metamaterials; pylon structure; ligament thickness; gait motion

I. INTRODUCTION

Prosthetic devices are designed to replace missing or amputated body parts and play a crucial role in restoring mobility and function [1]. Prosthetic development has increasingly incorporated control systems to enable active or semi-active behavior, such as the use of electric motors and Magnetorheological (MR) dampers [2, 3]. Active systems allow real-time adjustment through sensors and actuators, while semi-active MR dampers offer adaptive performance by modulating flow resistance via an applied magnetic field, making them particularly suitable for impact loading conditions or variable stiffness (k) applications [4, 5]. Despite these advantages, such systems require onboard power sources [6] and often increase both manufacturing and maintenance costs. Other developments in prosthetic design have focused on improving comfort and functionality through passive mechanical solutions [7, 8]. In Below-Knee Amputation (BKA) prosthetics [7], innovation has primarily focused on the pylon, introducing internal stiffness and damping characteristics that enable energy storage and shock absorption. These improvements enhance biomechanical efficiency, reduce impact forces during walking, and improve the swing phase of gait. In contrast, research on Above-Knee Amputation (AKA) prosthetics [8] has emphasized socket design, employing combinations of rigid and flexible materials to improve pressure distribution, enhance user comfort, and reduce the risk of secondary musculoskeletal conditions such as scoliosis. Although these studies focus on different prosthetic components, the pylon for BKA and the socket for AKA, they collectively highlight the importance of integrating mechanical design, material selection, and ergonomic considerations to improve prosthetic performance and life quality for amputees.

On the other hand, auxetic metamaterials can potentially be fine-tuned for specific functions within a purely mechanical system. In this system, components and sub-systems, such as springs or similarly behaving parts [9], act as actuators by storing input energy temporarily before releasing it as the input force recedes. A four-bar linkage mechanism has also been shown to provide a certain degree of motion to the prosthetics [10]. A more advanced design uses the foot itself to store and release energy, known as Energy Storage and Return (ESAR) [11]. For this design, carbon fiber is often chosen for its lightweight and high-strength properties. However, using carbon fiber affects manufacturing costs, leading to higher market prices and reducing accessibility for the general population. As an actuator for prosthetics, auxetic metamaterials have yet to be developed. Some implementations of auxetic metamaterials have been utilized for mechanical energy absorption in the foot component of a prosthetic device. Research has also focused on improving user comfort by applying auxetic metamaterials to the surface of the socket (interface part) of lower limb prosthetics [12]. Neither of these approaches uses auxetic metamaterials as an actuator; instead, they serve more as mechanical dampers to dissipate energy. This gap presents an opportunity for auxetic metamaterials to be used as actuators in prosthetics, especially in ESAR systems, due to their unique deformation behavior. It may be possible to replace springs with auxetic materials, given that the former exhibit a near-zero Poisson's ratio and are more likely to deform axially than laterally.

Metamaterials are a class of artificial materials with unique properties, combining their inherent material properties and the structure's design [13]. Their properties, such as a negative Poisson's ratio, which defines the negative ratio between lateral strain and axial strain, with a few exceptions, cannot be found in natural materials [14]. Metamaterials are classified according to their properties as optical (negative refraction index) [15], electromagnetic (negative permittivity) [16], thermal (negative thermal expansion) [17], acoustic (soundwave absorption) [18], and mechanical metamaterials [19]. Naturally occurring materials are likely to have a positive Poisson's ratio value, contributed by the tendency to thin under tensile and expand in a lateral direction under compression. In contrast, auxetic metamaterials made from the same inherent material would tend to expand under tensile stress and contract inward under compression [20]. Auxetic metamaterials have been proposed and discussed as beneficial in protective devices, robotics, and the medical field [21-23] developments. The development of auxetic metamaterials is generally divided into three categories. The first and most common is developing a novel structure [24] and improving certain aspects of already developed structures, such as increasing k [25]. Secondly, research is specifically conducted to improve the quality of fabricating auxetic metamaterials [26]. The third category is research aimed at applying auxetic metamaterials to functioning tools, for

instance, the implementation of a honeycomb sandwich panel to improve ballistic protections or implementation on the foot part of lower limb prosthetics [27, 28]. The auxetic re-entrant ligament structure allows the stiffness of the pylon to be adjusted by changing the ligament thickness, providing adaptability to different user requirements. This feature can significantly enhance user comfort and accommodate different activity levels, which is often a limitation in conventional prosthetics. The negative Poisson's ratio exhibited by the re-entrant auxetic structure enables increased deformation and effective energy dissipation during impact, especially during the gait cycle. This absorption is particularly beneficial for reducing peak loads transferred to the residual limb, enhancing the pylon's shock-absorbing capability compared to traditional designs. These benefits are unique to auxetic metamaterials and address specific challenges in prosthetic design, contributing to improved comfort, functionality, and user satisfaction.

Despite the growing number of studies exploring the use of auxetic metamaterials in rehabilitation applications, experimental validation of the performance of auxetic-based prosthetic devices remains limited. Accordingly, the primary technical contribution of this study is the design of a transtibial prosthetic pylon incorporating auxetic metamaterials, along with experimental validation of its mechanical performance. FEA is employed during the design process to address challenges associated with complex geometries and the lack of well-established constitutive models for metamaterials. The former provides an effective framework for investigating the mechanical behavior of auxetic structures, facilitating both the development of novel geometries and the evaluation of their performance within functional devices and systems. To address fabrication challenges associated with complex auxetic geometries, Additive Manufacturing (AM) techniques, specifically Fused Deposition Modeling (FDM), are utilized [29]. Although AM methods exhibit limitations in accurately reproducing the flexible behavior of auxetic metamaterials [30], these limitations can be assessed and mitigated through experimental testing, with key geometrical parameters informed by the FEA results. The specific aim of this work is to implement auxetic metamaterials as passive actuators within a novel transtibial prosthetic pylon. The proposed design is analyzed numerically using FEA and subsequently validated through experimental testing. In addition, the energy absorption performance of the auxetic pylon is compared with that of a conventional spring-based system. Finally, the study evaluates the practical feasibility of employing auxetic metamaterials as actuators in transtibial prosthetics and other rehabilitation devices.

II. MATERIALS AND METHODS

A. Pylon Design

An ordinary transtibial prosthetic pylon typically consists of a single rigid cylinder shell, functioning as a physical connection between the socket and the foot part of a prosthetic. Due to its apparent rigidity, this design provides no force damping, leading to a total k behavior, making it uncomfortable for the user. An alternative design, known as a telescopic pylon, deals with this k by adding a spring at one end of the cylinder. This spring will provide the needed flexibility to dampen some of the reaction force exerted during usage. This design was also developed into a damper system by replacing the spring with a full fluid-based damper system. As expected, this design offers the most control over how much force is needed to dissipate the reaction force. However, the need for fluid within the pylon would require a higher complexity during maintenance.

Figure 1 illustrates the geometries of the auxetic metamaterial structures considered in this study. The first configuration (Figure 1(a)) is derived from a planar 2D re-entrant hexagonal structure that is transformed into a 3D form by radially arranging each ligament to function as a pillar [29]. The second configuration (Figure 1(b)) is based on a fully 3D re-entrant hexagon structure reported in [31], which exhibits a negative Poisson's ratio in all principal directions. Inspired by this design, Figure 1(c) presents a modified orientation of the original re-entrant hexagon arranged into a radial 3D array, which forms the basis of the proposed auxetic structure. In conventional transtibial prosthetic design, the pylon typically consists of a rigid cylindrical component intended to maintain structural integrity during use. However, due to its high stiffness (k), such a design provides minimal energy absorption. To address this limitation, the proposed auxetic structure, shown in Figure 1(c), is incorporated into a novel auxetic metamaterial-based pylon, replacing the conventional rigid pylon, illustrated in Figure 2(a). The resulting pylon design, depicted in Figure 2(b), consists of three main components with a total length (L) of 10 cm. The design assumes a standard BKA, in which approximately 50% of the original limb length (assumed to be 20 cm) has been amputated. The upper component serves as the interface between the pylon and the prosthetic socket. Although a dedicated joint or connector may be included in future designs, the socket itself was not modeled in this study to ensure a flat surface suitable for experimental testing. In addition to providing socket attachment, the upper component maintains alignment of the structure by incorporating slots for inserting the ligaments of the middle component. The latter functions as the primary load-bearing element and accommodates the auxetic structure. It comprises eight bent ligaments oriented at a specified angle and positioned between the upper and lower components. The lower component mirrors the design of the upper component by providing corresponding slots for ligament insertion. Furthermore, it includes a central shaft designed to limit ligament displacement (S) and prevent structural collapse under excessive loading. A spherical feature at the top of the shaft matches the diameter of the hole in the upper component, ensuring proper alignment and stability during operation.

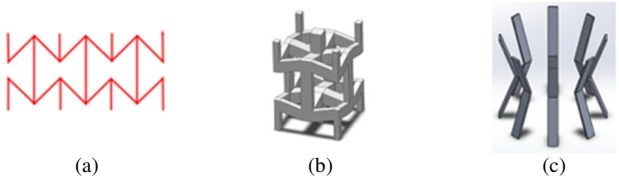

(a) (b) (c)

Fig. 1. Examples of metamaterial-based structures: (a) design parameters of the reoriented 3D re-entrant hexagonal unit cell, (b) design model of the modified 3D re-entrant structure, and (c) the proposed modified re-entrant hexagon arranged in a 3D radial configuration.

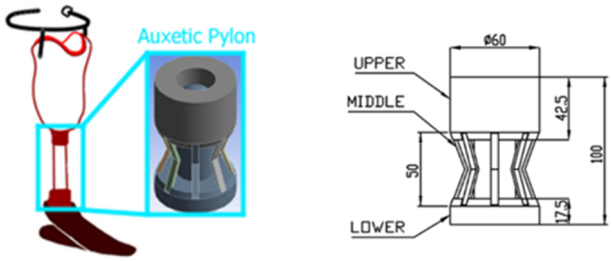

(a) (b)

Fig. 2. Proposed auxetic pylon design placement: (a) a schematic of the transtibial prosthetic, (b) the geometries along with the indication for upper, middle, and lower components.

Compared to conventional designs, the proposed pylon provides flexibility like that of a telescopic pylon, enabling damping through structural deformation while offering a simpler manufacturing process than spring-based systems. Unlike fluid-based pylon dampers, which can achieve high efficiency but require complex components and maintenance, the proposed design maintains mechanical simplicity and ease of maintenance. From a mechanical perspective, the pylon can be idealized as a single-degree-of-freedom spring system, in which each ligament within the middle component functions as an individual spring element, as illustrated in Figure 3(a) and further simplified in Figure 3(b). In this configuration, the auxetic bowtie structures primarily deform through the rotational motion of their arms about a central node. This rotation induces effective stretching or compression of the structure in response to an applied load. When a tensile force (F) is applied, the arms of the bowtie rotate outward, producing a vertical displacement (ΔL) and a corresponding horizontal displacement (ΔW). For small rotation angles, the resulting horizontal strain (ϵ_x) can be approximated as:

$$\epsilon_x = \frac{\Delta W}{W} \quad (1)$$

The vertical strain (ϵ_y) correlates with the ϵ_x due to Poisson's effect:

$$\epsilon_y = \frac{\Delta L}{L} \quad (2)$$

where L is the length of the bowtie, and W is its width. Then, the effective Young's modulus (E_{eff}) can be expressed by the correlation of the stress-strain. The applied stress (σ) in the vertical direction correlates to the force and the cross-sectional area (A) that is defined by the W and the thickness (t):

$$\sigma = \frac{F}{A} \quad (3)$$

$$\sigma = \frac{F}{(tW)} \quad (4)$$

Thus, the ϵ_y due to the rotation of the arms could use (2) by assuming that the rotation angle (θ) is small. Then $\Delta L \approx L\theta$. α was the geometric factor that accounts for the amplification due to the auxetic structure. This factor can be derived based on the specific geometry of the bowtie, but for simplification, it was assumed to be constant:

$$\epsilon_{eff} = \alpha \epsilon_y \quad (5)$$

The E_{eff} is the ratio of the σ to the effective strain:

$$E_{eff} = \frac{\sigma}{\epsilon_{eff}} \quad (6)$$

$$E_{eff} = \frac{\frac{F}{tW}}{\alpha\frac{\Delta L}{L}} = \frac{FL}{\alpha tW\Delta L} \quad (7)$$

Given that $\Delta L = L\theta$:

$$E_{eff} = \frac{F}{\alpha tW\theta} \quad (8)$$

By assuming a specific correlation for θ in terms of the σ and geometric parameters, we can further simplify and assume that θ is proportional to F, then:

$$\theta = \beta F \quad (9)$$

$$E_{eff} = \frac{1}{\alpha\beta tW} \quad (10)$$

where α is the geometric amplification factor, and β is the constant relating θ to σ. The k of a structure is a measure of its resistance to S under σ. For 2D auxetic metamaterials with a bowtie structure, k can be modeled by considering its geometric configuration and how it deforms under σ. Thus, using the force-displacement correlation, the equation for F could be expressed as:

$$F = k\Delta L \quad (11)$$

To determine k, the correlation between F and the displacement was required to take into consideration the geometry of the bowtie. ΔL correlates with $\Delta\theta$ and L ($\Delta L \approx L\Delta\theta$). Thus, the rotational stiffness ($k\theta$) could be expressed as:

$$F = k_\theta \Delta\theta \quad (12)$$

$$F = k_\theta \frac{\Delta L}{L} \quad (13)$$

$k\theta$ depends on the properties and geometry of the material. Therefore, for small S:

$$k_\theta \approx \frac{E_0 I}{r} \quad (14)$$

where, E_0 is the Young's modulus of the base material, I is the moment of inertia of the arms of the bowtie, and r is the distance from the center of the rotation to the point where F was applied. r is approximately half the L of the bowtie ($L/2$). The I for a rectangular A is:

$$I = \frac{tW^3}{12} \quad (15)$$

The correlation between the E_{eff} of the 2D auxetic bowtie metamaterial and the base material's E_0 is given by (16). Then, the equation for k is given by:

$$E_{eff} = \frac{E_0 W^2}{6L} \quad (16)$$

$$k = \frac{E_0 tW^3}{6L^2} \quad (17)$$

Or:

$$k = \frac{E_{eff} tW}{L} \quad (18)$$

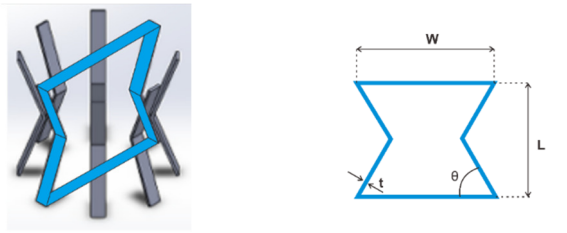

(a) (b)

Fig. 3. Schematic configuration and geometry: (a) the proposed design configuration from the sides, (b) the simplified diagram illustrating the arrangement of the pylon and its ligaments.

B. Material Consideration

Based on the assumption that the ligaments in the middle component function as spring-like elements, an appropriate material with high elasticity and strength was required. Accordingly, high-carbon spring steel plate grade SK5 was selected for the ligaments. In contrast, the upper and lower components were fabricated from Polylactic Acid (PLA), chosen for its low weight and compatibility with AM techniques, particularly FDM. The PLA components were manufactured using a Creality® Ender-3 printer with an infill density of 30% [31]. This infill density was selected to balance structural strength and lightweight performance. The mechanical properties of PLA are summarized in Table I [31].

TABLE I. MECHANICAL PROPERTIES OF PLA

Mechanical properties	Parameters
Density (g/cm³)	1.24
Young's modulus (MPa)	3420
Poisson's ratio	0.3
Elongation at break (%)	4.2

TABLE II. MECHANICAL PROPERTIES OF SK5 SPRING STEEL

Mechanical properties	Parameters
Young's modulus (GPa)	208
Yield strength (MPa)	1240

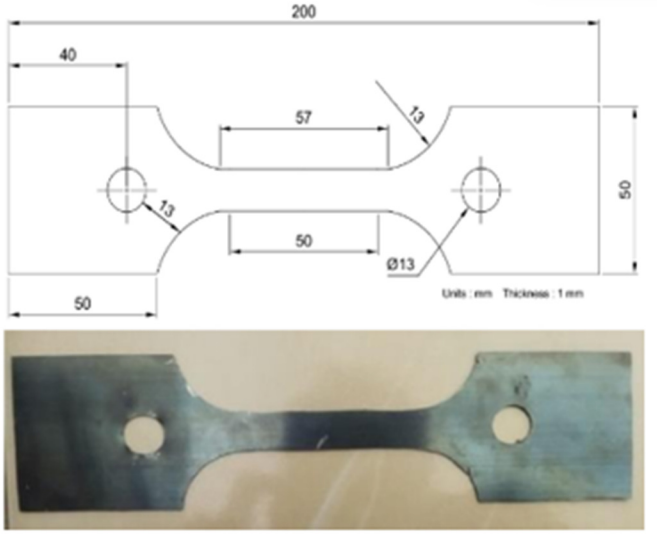

Fig. 4. Schematic and photograph of ASTM E8 pin-loaded specimen.

To accurately characterize the mechanical behavior of the SK5 spring steel used in the ligaments (Table II), tensile testing was conducted in accordance with [32], using a pin-loaded specimen geometry. The testing setup and specimen configuration are displayed schematically and photographically in Figure 4. The resulting mechanical response is presented in Figure 5 in terms of force–displacement (Figure 5(a)) and stress–strain (Figure 5(b)) relationships.

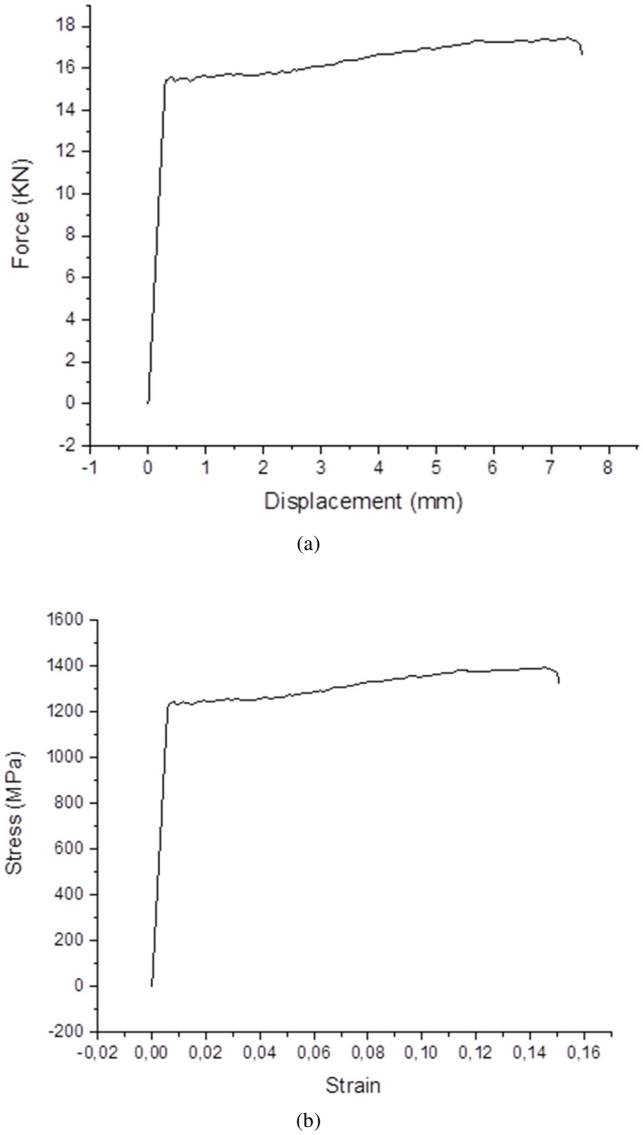

(a)

(b)

Fig. 5. Results of tensile testing in terms of: (a) force-displacement and (b) stress-strain.

C. Experimental Validation

The FEA results were experimentally validated by testing a physical prototype under identical loading conditions (ΔL = 4 mm). The prototype fabrication was carried out in three stages: manufacturing the upper and lower components, fabricating the middle ligament component, and assembling the complete pylon. For the upper and lower components, 3D models were

created and exported in Standard Tessellation Language (STL) format for slicing using Ultimaker® Cura 5.3. These parts were then produced via FDM-based 3D printing. Following fabrication, the printed components were inspected for dimensional accuracy and surface defects. Minor fitting issues, such as surface roughness, were corrected through sanding. Attention was given to ensuring smooth sliding contact between the inner surface of the upper component and the spherical head of the lower shaft, to prevent frictional effects from influencing the experimental response of the ligaments. The middle component ligaments were fabricated by cutting rectangular profiles from SK5 spring steel plates with thicknesses of 0.3 mm, 1 mm, and 2 mm, enabling a comparative evaluation of stiffness (k) across different ligament thicknesses. Each ligament was then bent at a 40° angle at its center to form the auxetic configuration. Assembly of the pylon was performed by aligning the shaft of the lower component with the corresponding hole in the upper component, followed by inserting the ligaments into the designated slots in both the upper and lower parts. The ligaments were secured using a plastic steel adhesive applied to the slots to ensure firm attachment. The fully assembled prototype is shown in Figure 6. During the design phase, alternative joining methods were considered, including welding the ligaments to the upper and lower components in a manner analogous to a tubular vehicle chassis structure [33]. However, this approach was deemed undesirable due to the additional weight it would introduce. Consequently, welding was omitted, provided that the adhesive-bonded joints between the PLA components and the steel ligaments remained structurally intact.

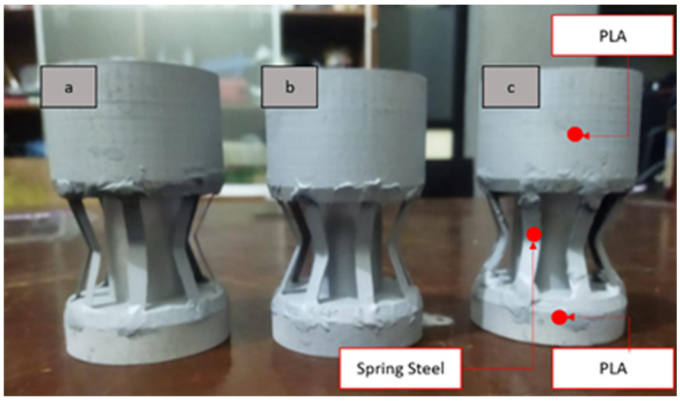

Fig. 6. Photograph of sample prototype for the proposed pylon design: (a) 0.3 mm, (b) 1 mm, (c) 2 mm.

The prototype was experimentally validated using an FEA model of a quasi-static press, namely a universal testing machine. The maximum total reaction force was measured utilizing a load cell during the compression procedure. A total of three samples were tested for validation.

D. Simulation Procedure

Geometrical models were first generated and then exported as Initial Graphics Exchange Specification (IGES) files into Ansys® Workbench. The contract definition of each part within the pylon assembly was defined based on the type of connection fabricated for the prototype. The fixed connection of ligaments and upper and lower parts was modeled as bonded connections to define a permanent connection between their surfaces. Meanwhile, the contact between the inner face of the ligaments and the surface of the lower shaft, along with the connection of the upper hole and the lower shaft, was defined with a frictional contact coefficient of 0.2. Following the contact definition, the model was meshed. Considering the priority of focusing on the behavior of the middle part compared to the other parts while also limiting the computational burden, a rather coarse value of 6mm was chosen for the upper and lower mesh elements. In comparison, considering the need to model the behavior of the middle part accurately, a mesh convergency analysis was conducted by varying the mesh element size with an identical model (t=0.3 mm), boundary condition (force load=686.6 N), and tracking its maximum ΔL starting with a coarse value of 1 mm and getting smoother until stabilizing at 0.3 mm (Table III) and compared in Figure 7. Based on the mesh convergence analysis, the resulting maximum ΔL stabilized at element size=0.3 mm, as shown by the minimum difference compared to 0.4mm. The general boundary condition for each simulation was defined as fixing the bottom surface of the lower part, limiting the displacement on the X and Z axes for the upper part, and defining the load on the top surface of the upper part. The complete simulation procedure, including the contact definition, meshing, and boundary conditions, is illustrated in Figure 8.

TABLE III. RESULTS OF THE MESH CONVERGENCE ANALYSIS OF THE LIGAMENTS OF THE MIDDLE PART

Element size	Number of elements	Max. displacement
1	5262	-4.407
0.9	5982	-4.4889
0.8	6910	-4.4977
0.7	7966	-4.4789
0.6	9582	-4.4755
0.5	11742	-4.4827
0.4	17038	-4.474
0.3	27310	-4.472

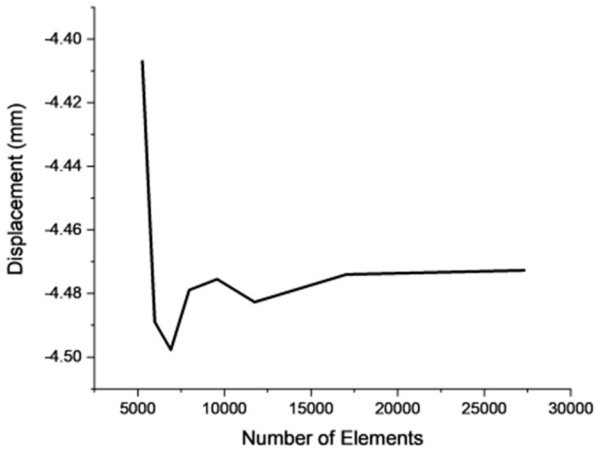

Fig. 7. Mesh convergence analysis results tracking the maximum vertical displacement with varying mesh element size over the number of elements within the model.

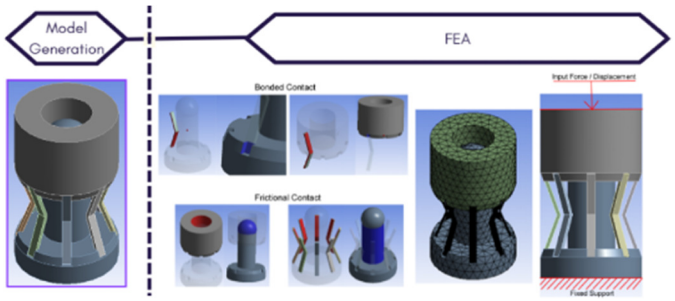

Fig. 8. Simulation procedure (FEA analysis) from model generation, contact definition, meshing configuration, and boundary condition (from left to right)

E. Case Definition

Two usage conditions for the pylon were simulated to analyze their behavior and performance during body weight bearing and during gait conditions. For body weight bearing, a load based on an assumption regarding the patient's body weight was defined on top of the upper part at 70 kg or 686.6 N. The weight was simulated in quasi-static conditions with linear loading. Meanwhile, the gait simulation condition was based on experimental conditions tracking the ground reaction force of five patient samples over time at a walking rate of 1.58 m/s, as illustrated in Figure 9 [34]. This gait behavior model was chosen because of its representation in terms of body-weight ratio rather than plain force. This, in turn, made it possible to assume a desirable body weight as required. The gait was divided into four stages: the loading response, midstance, terminal swing, and pre-swing.

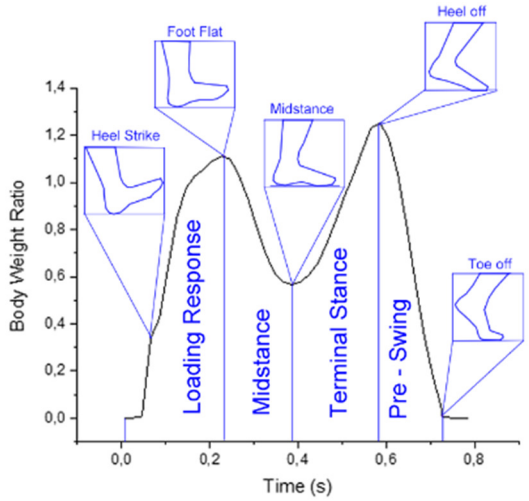

Fig. 9. Body weight ratio over time during gait of a patient walking with the rate of 1.58 m/s.

III. EXPERIMENTAL VALIDATION

Experimental testing, along with an equivalent simulation process, was conducted, with the results depicted in Figure 10. The results were compared in terms of reaction force over displacement. To quantify the difference in value, the error between the simulation and the experimental results can be calculated as:

$$\text{Error} = \left|\frac{(\bar{X}_{exp} - \bar{X}_{FEA})}{\bar{X}_{exp}}\right| \quad (19)$$

$$\text{Error} = 0.069 = 6.96\% \quad (20)$$

As portrayed in Figure 10, the experimental results exhibit good agreement with the FEA predictions, as evidenced by the similar trends in the force–displacement curves. The discrepancy between the experimental and numerical results was quantified as 6.96%. During the experimental testing, Digital Image Correlation (DIC) was employed to measure both axial and transverse displacements (S), which were subsequently compared with the corresponding FEA results (Figure 10). These displacement measurements were then used to calculate the Poisson's ratio of the system using the formulations presented above.

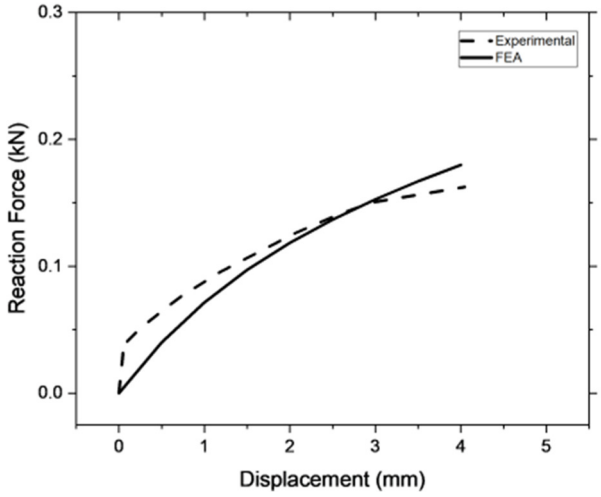

Fig. 10. Comparison of FEA and experimental results for validation.

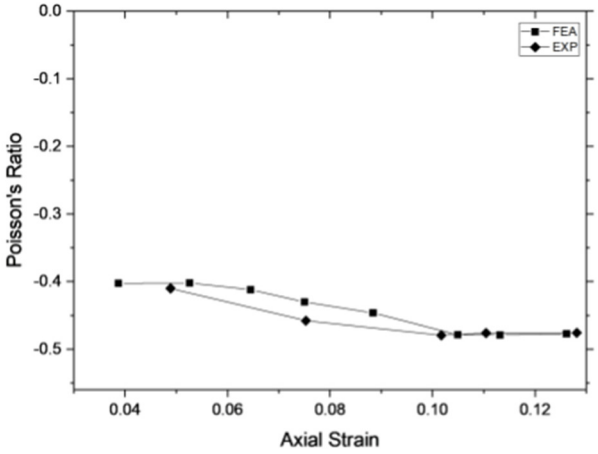

Fig. 11. Comparison of FEA and experimental results for validation in terms of the Poisson's ratio observed over axial strain during testing.

A comparison of the experimentally measured and numerically predicted Poisson's ratios is illustrated in Figure 11. Figure 12 demonstrates that the deformation behaviors observed experimentally closely match those obtained from the simulations. The deformation response can be divided into two

distinct stages. The first stage, referred to as the primary bending phase, is characterized by a reduction in the initial bend angle of the ligaments. This deformation continues until the ligaments meet the surface of the lower shaft. Upon contact, further deformation at the initial bend is constrained, triggering a second deformation stage, referred to as the secondary bending phase.

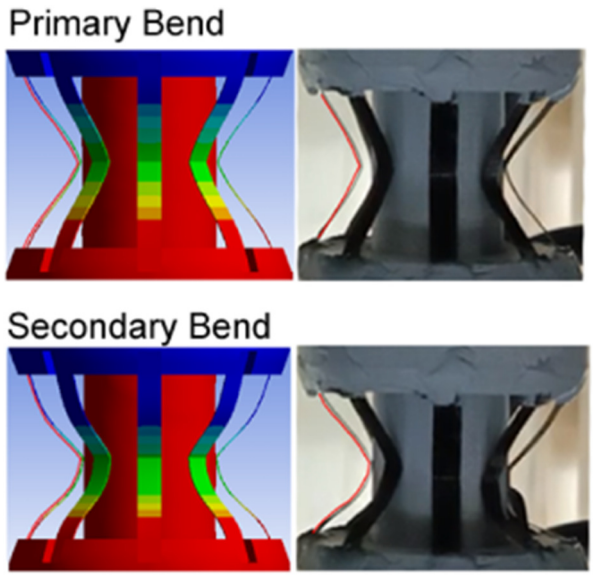

Fig. 12. Deformation comparison between experimental (right) and simulation results (left).

A. *Body Weight Case*

FEA was performed to simulate quasi-static load-bearing conditions for pylons with varying ligament thicknesses (t). The resulting force–displacement and stress–strain responses are presented in Figures 13 and 14, respectively. As shown in Figure 13, the pylon with a ligament thickness of 0.3 mm exhibited the largest displacement (4.47 mm) and the lowest reaction force (354.45 N). This indicates that the 0.3 mm-thick ligament effectively reduced the applied ground reaction force by 51.6%, relative to the input load of 686.6 N through structural deformation. In contrast, pylons with ligament thicknesses of 1 mm and 2 mm showed minimal displacement and no appreciable reduction in reaction force compared to the applied load. Figure 14 shows that the 0.3 mm-thick ligament also experienced the highest stress levels. This behavior is attributed to the reduced cross-sectional area (A), as described in (4), where a smaller area subjected to a constant load results in higher stress. Additionally, stress fluctuations were observed in the 0.3 mm-thick ligament due to localized stress concentrations arising from the contact with the lower shaft and the onset of secondary bending deformation, as illustrated in Figure 15.

Based on the force-displacement curve, the energy absorption capacity of each variation can be calculated as the Area Under the Curve (AUC) or mathematically written based on the force integral method, where F defines the force over the S as:

$$Energy\ Absorbed = \int F\, dS \quad (20)$$

The energy absorption during the simulation was then calculated and compared for each t variation (Figure 16). The 0.3 mm-thick ligament yielded the highest energy absorption. This aligns with the hypothesis that the pylon would be able to absorb energy by deforming. The structure would absorb more energy the more it deforms [23]. In terms of the Poisson's ratio, all t variations demonstrated a negative Poisson's ratio as expected from an auxetic structure (Figure 17).

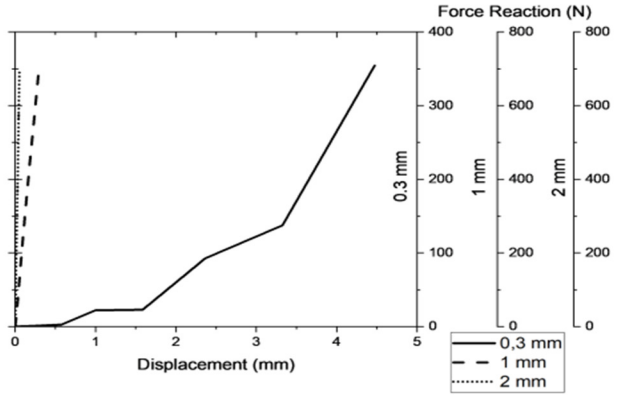

Fig. 13. Comparison of FEA results in terms of force reaction over axial displacement for 0.3 mm, 1 mm, and 2 mm of ligament thickness.

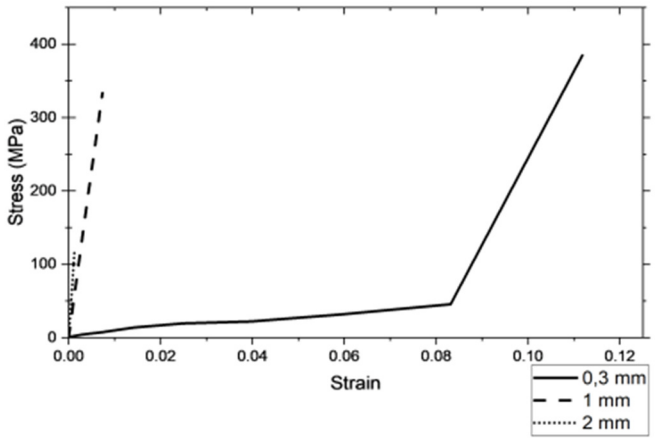

Fig. 14. Comparison of FEA results in terms of stress over axial strain for 0.3 mm, 1 mm, and 2 mm of ligament thickness.

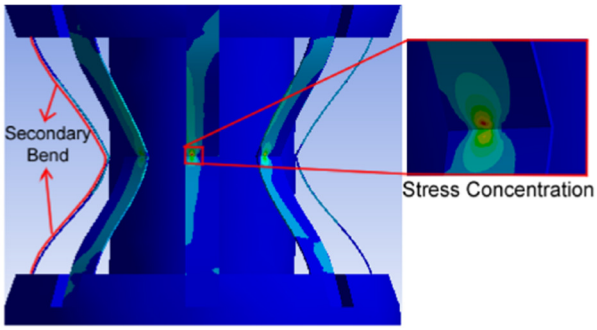

Fig. 15. The observed secondary bending mechanism was found on the ligament and stress concentration during contact with the lower shaft.

This also confirms that the negative Poisson's ratio of the original 2D model would remain, even if the design had been rearranged into a 3D model in a radial pattern. From Figure 17, it can also be seen that the 2 mm-thick ligaments experienced the highest average negative Poisson's ratio. To further analyze the actual Poisson's ratio of each t variation, a comparison of the Poisson's ratio over its axial strain was conducted (Figure 18). Although the 2 mm-thick ligaments experienced the highest average Poisson's ratio, the latter was caused by the minimum axial strain. It could be seen from the trend that the Poisson's ratio would rise as its axial strain increased. Thus, it can be argued that if the S was equal for each t, the Poisson's ratio value would not differ significantly. Table IV provides the k coefficients for the pylons.

TABLE IV. STIFFNESS COEFFICIENT FOR SYSTEM AND INDIVIDUAL LIGAMENT OF VARYING LIGAMENT THICKNESS

Ligament thickness (mm)	Stiffness coefficient (kN/mm)
0.3	1404
1	4680
2	9360

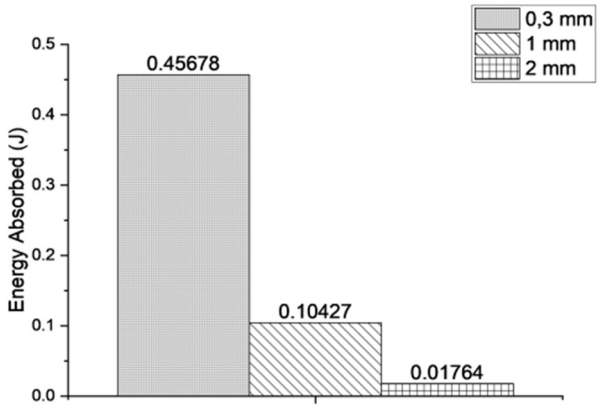

Fig. 16. Energy absorption for each ligament thickness variation.

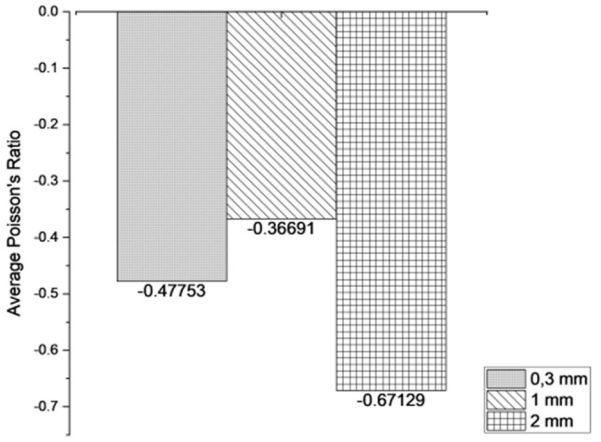

Fig. 17. Average Poisson's ratio for each thickness variation.

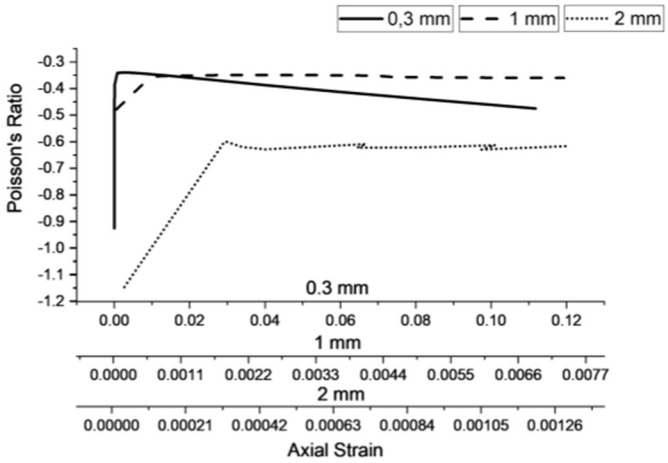

Fig. 18. Poisson's ratio over axial strain for each thickness variation.

B. Gait Simulation Case

A gait simulation was conducted to analyze the behavior of the proposed pylon under gait conditions. For comparison, a similar study was conducted experimentally to define the effect of different k on the behavior of the Shock-Absorbing Pylon (SAP) [24]. The k of the proposed pylon (Table IV) was then compared with commercially available SAP. The SAP is a modular prosthetic component specifically designed to reduce impact forces. Unlike traditional rigid pylons, SAPs can compress to absorb, return, or dissipate energy. It has been demonstrated that using a SAP can enhance comfort and reduce residual limb pain for lower-limb prosthesis users. While it is known that the longitudinal stiffness of a SAP influences gait kinematics, kinetics, and the overall work done by the lower limb, the energetic contributions of the prosthesis and intact joints have not been thoroughly investigated. The SAP design in the comparison performed in the present study aimed to evaluate how SAP stiffness and walking speed affect the mechanical work contributions of the prosthesis (comprising all components below the socket), knee, and hip in individuals with transtibial amputation. The referenced study provided data on mechanical work during the prosthesis' positioning and pylon compression phases at various stiffness levels and walking speeds, serving as a benchmark for assessing performance throughout the full gait cycle. The gait behavior of the proposed design and the standard SAP was evaluated under normal and rigid specifications, as illustrated in Figure 19 [6]. The auxetic pylon with a 1-mm-thick ligament exhibited significantly stiffer behavior than the normal SAP. This observation is consistent with the stiffness coefficient k, as the normal SAP shows a larger displacement Sunder the applied gait forces. Furthermore, the auxetic pylon with a 0.3-mm-thick ligament demonstrated an even greater deviation from the normal SAP, exhibiting a behavior that closely resembles that of a rigid SAP.

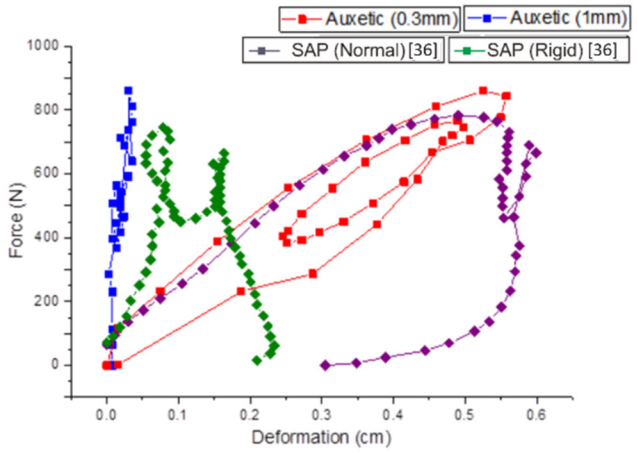

Fig. 19. Deformation comparison between the proposed Auxetic Pylon and the referenced SAP pylon with equivalent force applications.

Figure 20 depicts a more detailed breakdown of the gait simulation results of the auxetic pylon with a 0.3 mm-thick ligament. The gait cycle starts with a loading response, indicated by initial contact or heel strike (1), and this stage continues until the weight is fully loaded on the leg (2). By the end of the loading response, the *L* of the pylon decreased to 9.5 cm from its original 10 cm. In the next stage, as the weight was distributed more evenly, the *L* of the pylon retracted gradually as the force reaction decreased until it started the terminal stance (3). During the terminal stance, the *L* of the pylon was at its lowest (9.43 cm) during heel off (4), and then gradually decreased as the leg commenced its swing phase until all the weight was released as the leg was no longer in contact with the ground (5). The *L* of the pylon returned to its original *L* of 10 cm.

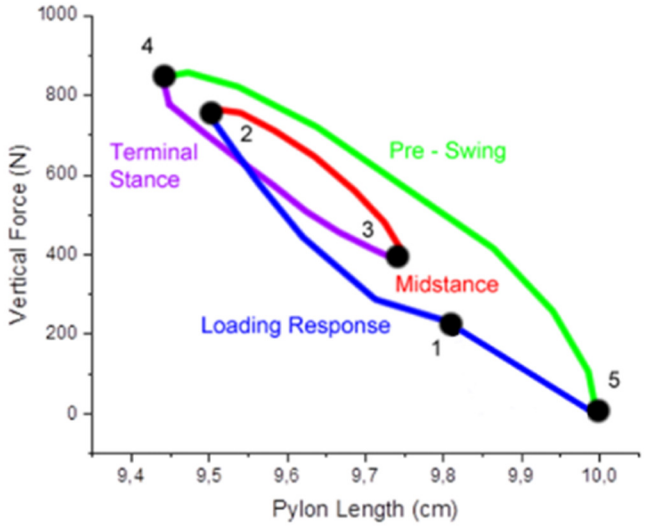

Fig. 20. Force over pylon length during gait simulation for 0.3 mm and 1 mm of ligament thickness.

Based on the data regarding the correlation between force reaction on both the energy absorption and reaction force (Figures 13 and Figure 16), it was gathered that the amount of S provided by the proposed design would dampen some of the reaction force and, in turn, absorb the exerted energy during a vertical press loading. A similar condition was also applied during gait, wherein as the person walks, the pylon will endure some form of S. By this assessment, the same behavior of energy absorption and reaction force damping was also expected. This result sufficed to compare that the proposed design would be able to function similarly to a telescopic pylon. Further research is needed for clinical assessment.

IV. CONCLUSIONS

In this study, a novel design methodology for a transtibial prosthetic pylon incorporating an auxetic metamaterial structure was developed and evaluated through both numerical simulations and experimental testing. In conventional prosthetic design, pylons are typically solid or tubular components, and damping characteristics are not explicitly considered. Instead, damping is usually provided by the prosthetic foot or by additional devices such as viscous dampers. In contrast, the proposed design integrates structural strength and damping functionality into a single pylon component. The design process consists of three main sections: an upper part that interfaces with the socket, a middle part that serves as the primary load-bearing region, and a lower part that connects to the prosthetic foot. The auxetic metamaterial was initially designed using a Two-Dimensional (2D) re-entrant hexagonal unit cell and subsequently transformed into a Three-Dimensional (3D) configuration. This resulted in eight ligament-like structures positioned between the upper and lower sections of the pylon. The performance of the proposed pylon was evaluated under two loading conditions, considering key parameters such as body weight and gait motion. The FEA results showed strong agreement with the experimental measurements, with a maximum deviation of 6.96%, thereby validating the accuracy of the numerical model. In addition, DIC confirmed the axial and transverse strain distributions observed during experimental testing. Experimental validation of the prototype pylon demonstrated the effectiveness of the proposed design methodology. Among the configurations tested, the pylon with a 0.3-mm-thick ligament exhibited the largest displacement (4.47 mm) and the lowest reaction force (354.45 N), corresponding to a 51.6% reduction in ground reaction force relative to the applied load of 686.6 N. This configuration also showed the highest energy absorption capability, attributed to its significant reduction in ground reaction force. Furthermore, during the terminal stance phase, the auxetic pylon with a 0.3-mm-thick ligament experienced a maximum length reduction of 5.7% (from 10 cm to 9.43 cm), indicating increased energy absorption associated with higher displacement *S*. The displacement behavior of the pylon can be characterized by primary and secondary bending mechanisms. The primary bending corresponds to the overall displacement *S* of the pylon, during which the initial bend angle of the ligament narrows under load. As deformation progresses, the ligament encounters the lower shaft, inducing a secondary bending response. These observations confirm the feasibility of implementing a 3D auxetic metamaterial structure, derived from a 2D re-entrant hexagonal geometry, which exhibits a negative Poisson's ratio. Overall, the proposed design methodology for transtibial prosthetic pylons utilizing auxetic

metamaterials is both simple and effective. The results suggest that a wide range of rehabilitation devices and systems, including prosthetic components, can be designed and manufactured using this approach with minimal modification. It should be noted, however, that this study focused solely on the pylon design and did not include full prosthetic assembly or clinical testing with human subjects. Consequently, future work should investigate fatigue behavior, impact loading, and long-term performance through comprehensive experimental and clinical evaluations.

ACKNOWLEDGMENT

The authors extend their appreciation to the Universitas Sebelas Maret, King Salman Center and Ministry of Higher Education, Science, and Technology of Indonesia (Kemendiktisaintek) for Disability Research for funding this work through International Collaboration 2025 research scheme (KI UNS 2025 no 369/UN27.22/PT.01.03/2025), Research Group no KSRG-2024-460 and Doctoral Program Completion Scholarship 2025.

REFERENCES

[1] C. Cipriani, M. Controzzi, and M. C. Carrozza, "Progress towards the development of the SmartHand transradial prosthesis," *2009 IEEE International Conference on Rehabilitation Robotics*, 2009, https://doi.org/10.1109/ICORR.2009.5209620.

[2] H. M. Herr and A. M. Grabowski, "Bionic ankle-foot prosthesis normalizes walking gait for persons with leg amputation," *Proceedings. Biological Sciences*, vol. 279, no. 1728, pp. 457–464, Feb. 2012, https://doi.org/10.1098/rspb.2011.1194.

[3] S. A. A. Aziz, Ubaidillah, S. A. Mazlan, N. I. N. Ismail, and S.-B. Choi, "Implementation of functionalized multiwall carbon nanotubes on magnetorheological elastomer," *Journal of Materials Science*, vol. 53, no. 14, pp. 10122–10134, July 2018, https://doi.org/10.1007/s10853-018-2315-3.

[4] A. Z. B. Pokaad, K. Hudha, and M. Z. B. M. Nasir, "Simulation and experimental studies on the behaviour of a magnetorheological damper under impact loading," *International Journal of Structural Engineering*, vol. 2, no. 2, pp. 164–187, Jan. 2011, https://doi.org/10.1504/IJStructE.2011.039422.

[5] F. Imaduddin, S. A. Mazlan, Ubaidillah, H. Zamzuri, and A. Y. A. Fatah, "Testing and parametric modeling of magnetorheological valve with meandering flow path," *Nonlinear Dynamics*, vol. 85, no. 1, pp. 287–302, July 2016, https://doi.org/10.1007/s11071-016-2684-6.

[6] J. A. Maun, S. A. Gard, M. J. Major, and K. Z. Takahashi, "Reducing stiffness of shock-absorbing pylon amplifies prosthesis energy loss and redistributes joint mechanical work during walking," *Journal of Neuroengineering and Rehabilitation*, vol. 18, no. 1, Sept. 2021, Art. no. 143, https://doi.org/10.1186/s12984-021-00939-8.

[7] M. R. Ismail, Y. Y. Kahtan, and S. M. Abbas, "A modified shank for below knee prosthesis," *IOP Conference Series: Materials Science and Engineering*, vol. 671, no. 1, Jan. 2020, Art. no. 012061, https://doi.org/10.1088/1757-899X/671/1/012061.

[8] H. S. Hasan, S. M. Abbas, S. K. Mohammed, and M. Q. Ibraheem, "Modeling and Manufacturing of a Flexible Socket for Above-Knee Amputation Prosthesis," *Engineering, Technology & Applied Science Research*, vol. 15, no. 2, pp. 21257–21262, Apr. 2025, https://doi.org/10.48084/etasr.10046.

[9] C. W. Radcliffe, "Four-bar linkage prosthetic knee mechanisms: Kinematics, alignment and prescription criteria," *Prosthetics and Orthotics International*, vol. 18, no. 3, pp. 159–173, Dec. 1994, https://doi.org/10.3109/03093649409164401.

[10] H. Houdijk, D. Wezenberg, L. Hak, and A. G. Cutti, "Energy storing and return prosthetic feet improve step length symmetry while preserving margins of stability in persons with transtibial amputation," *Journal of Neuroengineering and Rehabilitation*, vol. 15, no. Suppl 1, Sept. 2018, Art. no. 76, https://doi.org/10.1186/s12984-018-0404-9.

[11] M. Kowalczyk and H. Jopek, "Numerical Analysis of the Lower Limb Prosthesis Subjected to Various Load Conditions," *Vibrations in Physical Systems*, vol. 31, 2020, Art. no. 20203091, https://doi.org/10.21008/J.0860-6897.2020.3.09.

[12] M. F. Fardan, B. W. Lenggana, U. Ubaidillah, S.-B. Choi, D. D. Susilo, and S. Z. Khan, "Revolutionizing Prosthetic Design with Auxetic Metamaterials and Structures: A Review of Mechanical Properties and Limitations," *Micromachines*, vol. 14, no. 6, June 2023, Art. no. 1165, https://doi.org/10.3390/mi14061165.

[13] C. Lees, J. F. V. Vincent, and J. E. Hillerton, "Poisson's Ratio in Skin," *Bio-Medical Materials and Engineering*, vol. 1, no. 1, pp. 19–23, Feb. 1991, https://doi.org/10.3233/BME-1991-1104.

[14] J. B. Pendry, "Negative Refraction Makes a Perfect Lens," *Physical Review Letters*, vol. 85, no. 18, pp. 3966–3969, Oct. 2000, https://doi.org/10.1103/PhysRevLett.85.3966.

[15] J. B. Pendry, A. J. Holden, W. J. Stewart, and I. Youngs, "Extremely Low Frequency Plasmons in Metallic Mesostructures," *Physical Review Letters*, vol. 76, no. 25, pp. 4773–4776, June 1996, https://doi.org/10.1103/PhysRevLett.76.4773.

[16] S. Narayana and Y. Sato, "Heat Flux Manipulation with Engineered Thermal Materials," *Physical Review Letters*, vol. 108, no. 21, May 2012, Art. no. 214303, https://doi.org/10.1103/PhysRevLett.108.214303.

[17] Z. Liu *et al.*, "Locally Resonant Sonic Materials," *Science*, vol. 289, no. 5485, pp. 1734–1736, Sept. 2000, https://doi.org/10.1126/science.289.5485.1734.

[18] *Mechanics of Materials*. USA: McGraw-Hill, 2013.

[19] R. Lakes, "Foam Structures with a Negative Poisson's Ratio," *Science*, vol. 235, no. 4792, pp. 1038–1040, Feb. 1987, https://doi.org/10.1126/science.235.4792.1038.

[20] C. Qi, A. Remennikov, L.-Z. Pei, S. Yang, Z.-H. Yu, and T. D. Ngo, "Impact and close-in blast response of auxetic honeycomb-cored sandwich panels: Experimental tests and numerical simulations," *Composite Structures*, vol. 180, pp. 161–178, Nov. 2017, https://doi.org/10.1016/j.compstruct.2017.08.020.

[21] A. G. Mark, S. Palagi, T. Qiu, and P. Fischer, "Auxetic metamaterial simplifies soft robot design: 2016 IEEE International Conference on Robotics and Automation, ICRA 2016," *2016 IEEE International Conference on Robotics and Automation, ICRA 2016*, pp. 4951–4956, June 2016, https://doi.org/10.1109/ICRA.2016.7487701.

[22] H.-S. Kim, H.-J. Um, W. Hong, H.-S. Kim, and P. Hur, "Structural design for energy absorption during heel strike using the auxetic structure in the heel part of the prosthetic foot," in *2021 18th International Conference on Ubiquitous Robots (UR)*, July 2021, pp. 130–133, https://doi.org/10.1109/UR52253.2021.9494652.

[23] H. Yang, B. Wang, and L. Ma, "Mechanical properties of 3D double-U auxetic structures," *International Journal of Solids and Structures*, vol. 180–181, pp. 13–29, Dec. 2019, https://doi.org/10.1016/j.ijsolstr.2019.07.007.

[24] X. Li, Q. Wang, Z. Yang, and Z. Lu, "Novel auxetic structures with enhanced mechanical properties," *Extreme Mechanics Letters*, vol. 27, pp. 59–65, Feb. 2019, https://doi.org/10.1016/j.eml.2019.01.002.

[25] M. Bodaghi, A. Serjouei, A. Zolfagharian, M. Fotouhi, H. Rahman, and D. Durand, "Reversible energy absorbing meta-sandwiches by FDM 4D printing," *International Journal of Mechanical Sciences*, vol. 173, May 2020, Art. no. 105451, https://doi.org/10.1016/j.ijmecsci.2020.105451.

[26] W. Yang, R. Huang, J. Liu, J. Liu, and W. Huang, "Ballistic impact responses and failure mechanism of composite double-arrow auxetic structure," *Thin-Walled Structures*, vol. 174, May 2022, Art. no. 109087, https://doi.org/10.1016/j.tws.2022.109087.

[27] H.-J. Um, H.-S. Kim, W. Hong, H.-S. Kim, and P. Hur, "Design of 3D printable prosthetic foot to implement nonlinear stiffness behavior of human toe joint based on finite element analysis," *Scientific Reports*, vol. 11, no. 1, Oct. 2021, Art. no. 19780, https://doi.org/10.1038/s41598-021-98839-3.

[28] M. J. Mirzaali, S. Janbaz, M. Strano, L. Vergani, and A. A. Zadpoor, "Shape-matching soft mechanical metamaterials," *Scientific Reports*,

vol. 8, no. 1, Jan. 2018, Art. no. 965, https://doi.org/10.1038/s41598-018-19381-3.

[29] M. H. Zamani, M. Heidari-Rarani, and K. Torabi, "Optimal design of a novel graded auxetic honeycomb core for sandwich beams under bending using digital image correlation (DIC)," *Composite Structures*, vol. 286, Apr. 2022, Art. no. 115310, https://doi.org/10.1016/j.compstruct.2022.115310.

[30] L. Yang, O. Harrysson, H. West, and D. Cormier, "Mechanical properties of 3D re-entrant honeycomb auxetic structures realized via additive manufacturing," *International Journal of Solids and Structures*, vol. 69–70, pp. 475–490, Sept. 2015, https://doi.org/10.1016/j.ijsolstr.2015.05.005.

[31] J. M. Reverte, M. Á. Caminero, J. M. Chacón, E. García-Plaza, P. J. Núñez, and J. P. Becar, "Mechanical and Geometric Performance of PLA-Based Polymer Composites Processed by the Fused Filament Fabrication Additive Manufacturing Technique," *Materials*, vol. 13, no. 8, Jan. 2020, Art. no. 1924, https://doi.org/10.3390/ma13081924.

[32] *ASTM E8/E8M-22 Standard Test Methods for Tension Testing of Metallic Materials*. USA: ASTM International, 2024.

[33] H. Hazimi, U. Ubaidillah, R. Alnursyah, H. Nursya'bani, B. W. Lenggana, and Wibowo, "Improvement of Space Tube Frame for Formula Student Vehicle," in *Proceedings of the 6th International Conference and Exhibition on Sustainable Energy and Advanced Materials*, Singapore, 2020, pp. 735–744, https://doi.org/10.1007/978-981-15-4481-1_70.

[34] S. A. Gard and R. J. Konz, "The effect of a shock-absorbing pylon on the gait of persons with unilateral transtibial amputation," *Journal of Rehabilitation Research and Developmen*, vol. 40, no. 2, pp. 111–126, 2003.